The Synergistic Bactericidal Mechanism of Simultaneous Treatment with a 222-Nanometer Krypton-Chlorine Excilamp and a 254-Nanometer Low-Pressure Mercury Lamp

Jun-Won Kang,[a,b] Dong-Hyun Kang[a,b]

[a]Department of Food and Animal Biotechnology, Department of Agricultural Biotechnology, Center for Food and Bioconvergence and Research Institute for Agricultural and Life Sciences, Seoul National University, Seoul, Republic of Korea
[b]Institutes of Green Bio Science & Technology, Seoul National University, Pyeongchang-gun, Gangwon-do, Republic of Korea

ABSTRACT The purpose of this study was to investigate the synergistic bactericidal effect of 222-nm KrCl excilamp and 254-nm low-pressure (LP) Hg lamp simultaneous treatment against *Escherichia coli* O157:H7, *Salmonella enterica* subsp. *enterica* serovar Typhimurium, and *Listeria monocytogenes* in tap water and to identify the synergistic bactericidal mechanism. Sterilized tap water inoculated with pathogens was treated individually or simultaneously with a 254-nm LP Hg lamp or 222-nm KrCl excilamp. Overall, for all pathogens, an additional reduction was found compared to the sum of the log unit reductions of the individual treatments resulting from synergy in the simultaneous treatment with both kinds of lamps. In order to identify the mechanism of this synergistic bactericidal action, the form and cause of membrane damage were analyzed. Total reactive oxygen species (ROS) and superoxide generation as well as the activity of ROS defense enzymes then were measured, and the overall mechanism was described as follows. When the 222-nm KrCl excilamp and the 254-nm LP Hg lamp were treated simultaneously, inactivation of ROS defense enzymes by the 222-nm KrCl excilamp induced additional ROS generation following exposure to 254-nm LP Hg lamp (synergistic) generation, resulting in synergistic lipid peroxidation in the cell membrane. As a result, there was a synergistic increase in cell membrane permeability leading to a synergistic bactericidal effect. This identification of the fundamental mechanism of the combined disinfection system of the 222-nm KrCl excilamp and 254-nm LP Hg lamp, which exhibited a synergistic bactericidal effect, can provide important baseline data for further related studies or industrial applications in the future.

IMPORTANCE Contamination of pathogenic microorganisms in water plays an important role in inducing outbreaks of food-borne illness by causing cross-contamination in foods. Thus, proper disinfection of water before use in food production is essential to prevent outbreaks of food-borne illness. As technologies capable of selecting UV radiation wavelengths (such as UV-LEDs and excilamps) have been developed, wavelength combination treatment with UV radiation, which is widely used in water disinfection systems, is actively being studied. In this regard, we have confirmed synergistic bactericidal effects in combination with 222-nm and 254-nm wavelengths and have identified mechanisms for this. This study clearly analyzed the mechanism of synergistic bactericidal effect by wavelength combination treatment, which has not been attempted in other studies. Therefore, it is also expected that these results will play an important role as baseline data for future research on, as well as industrial applications for, the disinfection strategy of effective wavelength combinations.

KEYWORDS combined wavelengths, foodborne pathogens, synergistic effect mechanism, ultraviolet irradiation, water disinfection

Contaminated water is a major source of pathogenic microorganisms, which can pose a severe health threat to humans either by direct consumption or through its presence in washing food materials and food contact surfaces (1). In most developing countries, especially in rural areas, water safety is an important issue. According to the World Health Organization (WHO), contaminated water causes millions of deaths per year worldwide (2), and 663 million people still lacked access to improved drinking water sources in 2015 (3). Thus, it is of great significance to develop reliable water treatment technologies to effectively inactivate pathogenic microorganisms for human health and well-being (4).

UV irradiation can effectively inactivate various microorganisms in water and has been widely applied as a disinfection step in water treatment (4, 5). UV disinfection has numerous advantages, such as no disinfectant residuals, negligible formation of disinfection by-products (DBPs), no introduction of disinfectant resistance to bacteria, and facilitation for retrofitting into existing processes compared to conventional chemical treatments (6–9); thus, it has been recommended as a substitute for chemical additives to control pathogenic microorganisms in water (4, 10).

Among the features of UV technology, an attractive one is that it is possible to select a preferred wavelength which could be effectively applied to control a target pathogen as well as other specialized applications, because various monochromatic wavelengths can be produced according to UV source. Some typical UV sources capable of producing various wavelengths include UV light-emitting diodes (UV-LEDs) and discharge (DBD)-driven excimer lamps (excilamps). UV-LEDs are a source of UV radiation that can emit radiation from 210 nm to visible light depending on the semiconductor's bandgap (4, 11), and dielectric barrier excilamps can emit radiation from 74 to 354 nm depending on the type of rare gas and halogen used (12, 13). By using this feature, a hurdle technology can be applied that combines wavelengths exhibiting a synergistic effect on microbial inactivation due to different mechanisms involved in it (14). Consequently, through combination treatment representing the synergistic effect, it is possible to reduce the input energy by decreasing the treatment intensity required for reducing the pathogen to a desired level and also to ensure safety against pathogens by the increased inactivation effect (15, 16).

For this reason, many studies have been carried out on the synergistic effect of microbial inactivation by a combination of wavelengths (17–21). Among them, the inactivation effects of the wavelength combination treatments of 254/365 nm, 254/405 nm, and 280/365 nm using UV-LEDs (21), 254/365 nm using UV-LED and low-pressure (LP) Hg lamps (20), and 222/254 nm using an excilamp and an LP Hg lamp (17) were significantly higher than the sum of the inactivation effect of the individual treatments of each wavelength, proving that a synergistic effect occurs. On the other hand, the combination treatments of 265/280 nm, 265/310 nm, 280/310 nm, 265/280/310 nm (19), and 260/280 nm (18) using UV-LEDs and the combination treatment of 172/222 nm using an excilamp and an LP Hg lamp (17) did not show any synergistic effect. Thus, it has been demonstrated that both LED-UV and excilamps can generate a synergistic effect if combined appropriately. Meanwhile, most studies have focused on UV-LED combinations, and there is only one combination study involving excilamps. To date, in fact, most commercially available UV-C–LEDs produce an extremely low radiant output of less than 3 mW (22), and UV-LEDs with a range of 220 to 230 nm are not at a practical stage of development for application (18). However, the 222-nm wavelength excilamp has a greater bactericidal effect than the 254-nm LP Hg lamp, and excilamps have a sufficiently high output (23, 24). Therefore, a study involving a combined treatment system using KrCl excilamps, which have a high radiant power and a wavelength of 222 nm, is needed because it is likely to be applied in practice and, thus, enhance control of waterborne pathogens.

Although Ramsay et al. (17) demonstrated a synergistic effect with the combination of a 222-nm KrCl excilamp and 254-nm LP Hg lamp, the specific inactivation mechanism of this combination system has not yet been elucidated. Since understanding the technology's inactivation mechanisms not only helps to identify rate-limiting steps

TABLE 1 Log reductions of *E. coli* O157:H7 in tap water subjected to individual 254-nm LP Hg lamp, 222-nm KrCl excilamp, and simultaneous treatment

| Treatment time (s) | Log reduction [$\log_{10}(N_0/N)$][a] by treatment type and selection medium | | | | | |
| | 254-nm LP Hg lamp | | 222-nm KrCl excilamp | | Combined | |
	SMAC	SPRAB	SMAC	SPRAB	SMAC	SPRAB
0	0.00 ± 0.00 Aa	0.00 ± 0.00 Aa	0.00 ± 0.00 Aa	0.00 ± 0.00 Aa	0.00 ± 0.00 Aa	0.00 ± 0.00 Aa
1	0.39 ± 0.32 Aa	0.37 ± 0.22 Aa	0.29 ± 0.25 Aa	0.46 ± 0.35 Aa	2.51 ± 0.26 Bb	2.26 ± 0.41 Bb
3	1.47 ± 0.10 Ba	1.36 ± 0.27 Ba	1.99 ± 0.67 Ba	1.90 ± 0.23 Ba	5.05 ± 0.66 Cb	4.65 ± 0.69 Cb
5	1.71 ± 0.09 Ba	1.58 ± 0.30 Ba	3.30 ± 0.65 Cb	2.78 ± 0.37 Cb	7.59 ± 0.04 Dc	6.74 ± 0.26 Dd

[a]Values are means ± standard deviations from three replications. Means with different uppercase letters within the same column indicate significant differences ($P < 0.05$). Different lowercase letters within the same row indicate significant differences ($P < 0.05$). SMAC, sorbitol MacConkey agar; SPRAB, phenol red agar base with 1% sorbitol; N_0, initial population; N, population after treatment.

during processing with the system but also can facilitate the development of more effective inactivation strategies, the identification of the specific inactivation mechanism of this wavelength-combining system is of great significance (25). For this reason, we reaffirmed the synergistic effect of the 222-nm (KrCl excilamp) and 254-nm (LP Hg lamp) combination against major pathogenic bacteria (*Escherichia coli* O157:H7, *Salmonella enterica* subsp. *enterica* serovar Typhimurium, and *Listeria monocytogenes*) and identified the mechanism for this synergistic effect.

RESULTS AND DISCUSSION

Levels of *E. coli* O157:H7, *S.* Typhimurium, and *L. monocytogenes* in tap water after individual or simultaneous treatment with the 222-nm KrCl excilamp and 254-nm LP Hg lamp are presented in Tables 1, 2, and 3, respectively. For *E. coli* O157:H7, a significant difference ($P < 0.05$) in reduction levels between the two lamps occurred after 5-s treatments at equal doses of 1.05 mJ/cm² for the KrCl excilamp and 1.1 mJ/cm² for the LP Hg lamp. For *S.* Typhimurium and *L. monocytogenes*, the 222-nm KrCl excilamp resulted in significantly ($P < 0.05$) higher reduction levels than the 254-nm LP Hg lamp at all treatment times. Even though the radiation intensity of the 222-nm KrCl excilamp was slightly lower than that of the 254-nm LP Hg lamp (KrCl excilamp, 0.21 mW/cm²; LP Hg lamp, 0.22 mW cm²), higher reduction levels caused by the 222-nm KrCl excilamp at the same treatment time indicate that the 222-nm wavelength exhibited a greater bactericidal effect than the 254-nm wavelength. This is consistent with several previous studies, including our previous study in which 222-nm KrCl excilamps revealed a greater bactericidal effect than the 254-nm LP Hg lamp (11, 23, 26, 27). Based on our previous study identifying the inactivation mechanisms of the 222-nm KrCl excilamp, the results of the greater bactericidal effect of the 222-nm KrCl excilamp than the 254-nm LP Hg lamp are interpreted as follows. Since intracellular components such as lipids and proteins absorb more light at 222 nm than at a wavelength of 254 nm (whereas the 254-nm wavelength is absorbed more by DNA) and the 222-nm wavelength also generates intracellular reactive oxygen species (ROS), the 222-nm wave-

TABLE 2 Log reductions of *S.* Typhimurium in tap water subjected to individual 254-nm LP Hg lamp, 222-nm KrCl excilamp, and simultaneous treatment

| Treatment time (s) | Log reduction [$\log_{10}(N_0/N)$][a] by treatment type and selection medium | | | | | |
| | 254-nm LP Hg lamp | | 222-nm KrCl excilamp | | Combined | |
	XLD	OV-XLD	XLD	OV-XLD	XLD	OV-XLD
0	0.00 ± 0.00 Aa	0.00 ± 0.00 Aa	0.00 ± 0.00 Aa	0.00 ± 0.00 Aa	0.00 ± 0.00 Aa	0.00 ± 0.00 Aa
7	1.44 ± 0.57 Ba	1.18 ± 0.55 Ba	2.17 ± 0.60 Bb	1.17 ± 0.02 Ba	3.95 ± 0.78 Bc	3.33 ± 0.19 Bc
10	1.64 ± 0.33 Ba	1.76 ± 0.18 BCa	2.83 ± 0.45 BCb	1.78 ± 0.05 Ca	5.70 ± 0.40 Cc	4.39 ± 0.37 Cd
13	1.93 ± 0.38 Ba	1.96 ± 0.11 Ca	3.46 ± 0.18 Cc	2.79 ± 0.22 Db	6.42 ± 0.51 CDe	5.82 ± 0.39 Dd
15	1.98 ± 0.57 Ba	2.06 ± 0.24 Ca	3.58 ± 0.24 Cb	3.02 ± 0.45 Db	6.82 ± 0.16 Dc	6.95 ± 0.17 Ec

[a]Values are means ± standard deviations from three replications. Means with different uppercase letters within the same column indicate significant differences ($P < 0.05$). Different lowercase letters within the same row indicate significant differences ($P < 0.05$). XLD, xylose lysine desoxycholate agar; OV-XLD, overlay XLD agar on TSA; N_0, initial population; N, population after treatment.

TABLE 3 Log reductions of *L. monocytogenes* in tap water subjected to individual 254-nm LP Hg lamp, 222-nm KrCl excilamp, and simultaneous treatment

| Treatment time (s) | Log reduction [$\log_{10}(N_0/N)$][a] by treatment type and selection medium | | | | | |
| | 254-nm LP Hg lamp | | 222-nm KrCl excilamp | | Combined | |
	OAB	OV-OAB	OAB	OV-OAB	OAB	OV-OAB
0	0.00 ± 0.00 Aa	0.00 ± 0.00 Aa	0.00 ± 0.00 Aa	0.00 ± 0.00 Aa	0.00 ± 0.00 Aa	0.00 ± 0.00 Aa
7	0.62 ± 0.35 Ba	0.62 ± 0.17 Ba	1.06 ± 0.12 Bb	1.09 ± 0.11 Bb	2.75 ± 0.20 Bc	2.73 ± 0.12 Bc
10	0.78 ± 0.21 Ba	1.07 ± 0.10 Ca	1.70 ± 0.09 Cb	1.80 ± 0.35 Cb	4.18 ± 0.34 Cc	4.03 ± 0.47 Cc
13	1.31 ± 0.27 Ca	1.65 ± 0.30 Da	2.63 ± 0.44 Db	2.52 ± 0.39 Db	5.79 ± 0.06 Dc	5.54 ± 0.32 Dc
15	2.07 ± 0.06 Da	1.90 ± 0.04 Db	2.78 ± 0.40 Db	2.68 ± 0.43 Db	6.90 ± 0.23 Ec	6.58 ± 0.26 Ec

[a]Values are means ± standard deviations from three replications. Means with different uppercase letters within the same column indicate significant differences ($P < 0.05$). Different lowercase letters within the same row indicate significant differences ($P < 0.05$). OAB, Oxford agar base with antimicrobial supplement; OV-OAB, overlay OAB agar on TSA; N_0, initial population; N, population after treatment.

length affects simultaneously the cell membrane, enzymes, and DNA necessary to maintain cell viability, whereas the 254-nm wavelength affects only the DNA; thus, the 222-nm KrCl excilamp induces greater damage to pathogenic bacteria than the 254-nm LP Hg lamp. Specifically, the 222-nm wavelength inactivated respiratory chain dehydrogenase in the cell and induced lipid peroxidation of the cell membrane, leading to the formation of pores. Ha et al. (24) also confirmed that the 222-nm wavelength inactivated intracellular esterase and induced formation of cell membrane pores. Although the 222-nm wavelength induces destruction of DNA, it is not yet known what form of DNA damage occurs. On the other hand, it has been widely reported that the 254-nm wavelength induces several forms of DNA damage, including production of cyclobutane pyrimidine dimers (CPDs), pyrimidine(6–4)pyrimidine photoproducts, and DNA double- or single-strand breakage (20, 28–31).

The occurrence of sublethally injured cells after UV-C treatment should be considered, because they can be resuscitated under conditions that facilitate recovery and regain normal pathogenicity (32). As shown in Tables 1, 2, and 3, in the case of *E. coli* O157:H7 and *L. monocytogenes*, no injured cells were produced in any treatment except for simultaneous 5-s treatment of 222-nm KrCl excilamp and 254-nm LP Hg lamp at equal doses of 1.10 mJ/cm² for the LP Hg lamp and 1.05 mJ/cm² for the KrCl excilamp, whereas for *S.* Typhimurium, significant ($P < 0.05$) numbers of recovered cells occurred with the individual 222-nm KrCl excilamp treatment with 7 to 13 s of treatment at equal doses of 1.54 to 2.73 mJ/cm² and in the simultaneous 10 to 13 s of treatment with equal doses of 2.20 to 2.86 mJ/cm² for the LP Hg lamp and 2.10 to 2.73 mJ/cm² for the KrCl excilamp. This trend of cell recovery in *S.* Typhimurium following UV-C irradiation treatment has been reported in several studies (24, 33–35).

Meanwhile, simultaneous treatment with the 222-nm KrCl excilamp and 254-nm LP Hg lamp combination resulted in significantly greater ($P < 0.05$) reduction levels than the sum of the reduction levels generated by the individual treatments, except for the 7-s treatment (1.54 mJ/cm² for LP Hg lamp and 1.47 mJ/cm² for KrCl excilamp) of *S.* Typhimurium. This means that the combined treatment of the 222-nm KrCl excilamp and 254-nm LP Hg lamp produced a synergistic inactivation effect on the pathogens in tap water. Although this synergistic effect was already reported by Ramsay et al. (17), the results of our study are meaningful because we demonstrated the synergistic effects on major pathogenic bacteria that were not investigated by Ramsay et al. (17). Moreover, the mechanism for this synergistic effect had not previously been elucidated. Since it is necessary to identify the mechanism for effective practical application of this system, we sought to identify the mechanism for synergistic effect through several approaches.

The first step was to find the intracellular site where synergistic damage was induced by simultaneous treatment, because that is an important key for investigating the mechanism of the synergistic inactivation effect. Based on previous studies (23, 24) on the inactivation mechanism of the 222-nm KrCl excilamp, we assumed that the cell membrane, which exhibited remarkable damage following UV radiation treatment, is a

TABLE 4 PI uptake and lipid peroxidation values for cell membranes of *E. coli* O157:H7, *S. Typhimurium*, and *L. monocytogenes* subjected to individual or simultaneous 254-nm LP Hg lamp and 222-nm KrCl excilamp treatment[a]

Value[b] and treatment	Microorganism		
	E. coli O157:H7	*S.* Typhimurium	*L. monocytogenes*
PI uptake			
Untreated control	0.00 ± 0.00 A	0.00 ± 0.00 A	0.00 ± 0.00 A
254-nm LP Hg lamp	1.06 ± 1.20 A	1.12 ± 0.97 A	0.18 ± 0.17 A
222-nm KrCl excilamp	3.16 ± 0.19 B	4.20 ± 1.38 B	2.66 ± 1.57 B
LP Hg lamp + KrCl excilamp	7.92 ± 1.24 C	11.20 ± 1.37 C	12.49 ± 3.89 C
Lipid peroxidation of cell membrane			
Untreated control	0.00 ± 0.00 A	0.00 ± 0.00 A	0.00 ± 0.00 A
254-nm LP Hg lamp	67.3 ± 55.1 B	43.6 ± 7.5 B	24.3 ± 15.5 B
222-nm KrCl excilamp	441.3 ± 90.1 C	448.6 ± 33.0 C	302.6 ± 24.4 C
LP Hg lamp + KrCl excilamp	1,002.7 ± 233.4 D	869.3 ± 123.8 D	601.6 ± 96.2 D

[a]Values were obtained from PI uptake and DPPP assays.
[b]Values are means ± standard deviations from three replications. Means followed by different letters within the same column for each value are significantly different ($P < 0.05$). The data were normalized by subtracting fluorescence (OD_{600}) values obtained from untreated cells with the following formula: (fluorescence value after treatment − fluorescence value of untreated control)/OD_{600}.

site where synergistic damage occurred; thus, we examined cell integrity by means of the propidium iodide (PI) uptake assay. As shown in Table 4, the PI uptake value after simultaneous treatment with the 222-nm KrCl excilamp and 254-nm LP Hg lamp was significantly ($P < 0.05$) greater than the sum of the individual treatments. The increase in PI uptake value means that the permeability of the cell membrane increased due to the occurrence of physical damage, such as pore formation in the cell membrane, and this physical damage made it difficult for the cells to maintain homeostasis and eventually led to cell death (36, 37). Therefore, we deduce that the synergistic inactivation effect of simultaneous treatment is caused by synergistic damage to the cell membrane. Although we confirmed that the synergistic damage site was the cell membrane and physical damage occurred in the form of increased permeability, it remains questionable which component in the cell membrane underwent what form of change that eventually induced damage in the form of pore formation, resulting in increased permeability. For specific mechanism analysis, it was considered necessary to identify the cause of physical damage occurring in the cell membrane. Fatty acids are one of the most important building blocks of cellular components. They are mainly found in the cell membrane as the acyl constituent of phospholipids in bacterial cells (38). In particular, when peroxidation of lipids in the cell membrane occurs, cellular damages such as loss of fluidity, decreasing cell membrane potential, and increasing permeability occur and eventually lead to cell death (39). Based on this, we examined lipid peroxidation of the cell membrane by diphenyl-1-pyrenylphosphine (DPPP) assay, considering that the occurrence of lipid peroxidation in the cell membrane is the cause of physical damage to this organelle. As shown in Table 4, lipid peroxidation values of the cell membrane in cells subjected to simultaneous 222-nm KrCl excilamp and 254-nm LP Hg lamp treatment were significantly ($P < 0.05$) greater than the sum of values obtained from individual treatments. That is, simultaneous treatment with the 222-nm KrCl excilamp and 254-nm LP Hg lamp synergistically induced lipid peroxidation in the cell membrane, so it can be interpreted that physical membrane damage caused by simultaneous treatment with the two lamps was attributed to the occurrence of lipid peroxidation.

Since the site where the synergistic damage occurred in the cell and the cause of its occurrence have been identified, it is necessary to know what caused the damage. It is well established that UV radiation treatment causes ROS generation and, thus, oxidative damage to the cell (40–43). This is due to the principle that when cellular constituents such as chromophoric amino acids absorb UV irradiation, they generate excited-state species and radicals as a result of photoionization through the photosensitization

TABLE 5 Superoxide generation values within cells of *E. coli* O157:H7, *S.* Typhimurium, and *L. monocytogenes* subjected to individual or simultaneous 254-nm LP Hg lamp and 222-nm KrCl excilamp treatment[a]

	Microorganism		
Value[b] and treatment	*E. coli* O157:H7	*S.* Typhimurium	*L. monocytogenes*
Generation of superoxide (O_2^-)			
Untreated control	0.00 ± 0.00 A	0.00 ± 0.00 A	0.00 ± 0.00 A
254 nm LP Hg lamp	0.87 ± 1.84 A	1.63 ± 2.01 A	0.40 ± 0.55 A
222 nm KrCl excilamp	6.57 ± 1.39 B	10.99 ± 2.64 B	5.24 ± 0.66 B
LP Hg lamp + KrCl excilamp	15.34 ± 2.92 C	21.32 ± 1.15 C	13.55 ± 0.47 C
Generation of total ROS			
Untreated control	0.00 ± 0.00 A	0.00 ± 0.00 A	0.00 ± 0.00 A
254 nm LP Hg lamp	3.33 ± 3.33 A	8.88 ± 5.09 A	7.77 ± 3.85 A
222 nm KrCl excilamp	46.68 ± 3.33 B	46.67 ± 14.53 B	68.89 ± 10.72 B
LP Hg lamp + KrCl excilamp	120.00 ± 29.05 C	116.68 ± 3.33 C	190.00 ± 20.82 C

[a]Values were obtained using an HDE or CM-H2DCFDA probe.
[b]Values are means ± standard deviations from three replications. Means followed by different letters within the same column are significantly different ($P < 0.05$). The data were normalized by subtracting fluorescence (OD_{600}) values obtained from untreated cells as follows: (fluorescence value after treatment − fluorescence value of untreated control)/OD_{600}.

process (41, 44, 45). ROS are known to be one of the major causes of the activation of lipid peroxidation in cell membranes, leading to cell death by increasing cell membrane permeability (46–49). Thus, based on these facts, we hypothesized that the occurrence of ROS is related to the cause of synergistic damage in the form of lipid peroxidation. ROS are various forms of activated oxygen, including superoxide radicals, hydroxyl radicals, hydrogen peroxide, peroxyl, and peroxynitrite. Among them, superoxide (O_2^-), which is formed by adding one electron to an oxygen molecule, plays an important role in forming other oxygen radicals that have the potential to react with cell components and thereby induce damage (50–52). Thus, both the intracellular total ROS and superoxide generation were measured after simultaneous or individual treatment with the 222-nm KrCl excilamp and 254-nm LP Hg lamp. As shown in Table 5, interestingly, the degree of generation of both total ROS and superoxide within the cell after simultaneous treatment with the 222-nm KrCl excilamp and the 254-nm LP Hg lamp was significantly ($P < 0.05$) greater than the sum of that generated after individual treatment with the two lamps. Therefore, it can be interpreted that simultaneous treatment with the 222-nm KrCl excilamp and 254-nm LP Hg lamp synergistically generates ROS, which synergistically induces lipid peroxidation in the cell membrane, causing physical damage in the form of increased permeability. Eventually, simultaneous treatment causes a synergistic bactericidal effect by this chain reaction. Unsaturated fatty acids in particular are sensitive to the occurrence of peroxidation, because double bonds in fatty acids facilitate the removal of hydrogen ions by weakening the C-H bonds adjacent to the double bond; for this reason, unsaturated fatty acids in the cell membrane are more vulnerable to damage caused by ROS than saturated fatty acids (39, 53). Thus, it is postulated that the ROS generated in this study induced lipid peroxidation mostly in the unsaturated fatty acids in the cell membrane, resulting in damage. Although our study confirmed only lipid peroxidation of the cell membrane by ROS, it is believed that the produced ROS caused damage to cell constituents other than lipids, leading to a bactericidal effect, because ROS can cause oxidative damage not only to lipids but also to constituents such as proteins and DNA in many other microorganisms (54–57). Meanwhile, in order to complete the identification of the mechanism of the synergistic bactericidal action resulting from simultaneous treatment with both lamps, there still remains a question as to why ROS is synergistically generated by simultaneous treatment.

Organisms with aerobic metabolism have been known to generate ROS in normal metabolic processes as a by-product; thus, these organisms always face the risk of oxidative damage by this ROS. To protect themselves from this risk, aerobic organisms

TABLE 6 Values of SOD, CAT, and GPx inactivation for *E. coli* O157:H7, *S.* Typhimurium, and *L. monocytogenes* subjected to individual or simultaneous 254-nm LP Hg lamp and 222-nm KrCl excilamp treatment[a]

Value[b] and treatment	Microorganism		
	E. coli O157:H7	*S.* Typhimurium	*L. monocytogenes*
Inactivation of SOD			
Untreated control	0.00 ± 0.00 A	0.00 ± 0.00 A	0.00 ± 0.00 A
254 nm LP Hg lamp	0.02 ± 0.04 A	0.03 ± 0.03 A	0.02 ± 0.03 A
222 nm KrCl excilamp	0.09 ± 0.01 B	0.11 ± 0.01 B	0.11 ± 0.03 B
LP Hg lamp + KrCl excilamp	0.12 ± 0.04 B	0.11 ± 0.02 B	0.13 ± 0.01 B
Inactivation of CAT			
Untreated control	0.00 ± 0.00 A	0.00 ± 0.00 A	0.00 ± 0.00 A
254 nm LP Hg lamp	6.33 ± 5.86 A	12.67 ± 11.59 A	8.33 ± 4.04 A
222 nm KrCl excilamp	39.33 ± 3.79 B	110.00 ± 9.00 B	28.67 ± 6.11 B
LP Hg lamp + KrCl excilamp	47.00 ± 6.24 B	127.00 ± 3.61 B	39.00 ± 7.21 B
Inactivation of GPx			
Untreated control	0.00 ± 0.00 A	0.00 ± 0.00 A	0.00 ± 0.00 A
254 nm LP Hg lamp	113.33 ± 26.76 B	106.00 ± 11.79 B	86.00 ± 10.58 B
222 nm KrCl excilamp	491.67 ± 98.28 C	610.67 ± 71.62 C	494.67 ± 36.07 C
LP Hg lamp + KrCl excilamp	623.00 ± 27.07 D	709.67 ± 17.62 D	635.67 ± 33.50 D

[a]Values were obtained from SOD assay.
[b]Values are means ± standard deviations from three replications. Means followed by different letters within the same column for each value are significantly different ($P < 0.05$). The data were normalized by subtracting absorbance or fluorescence (OD_{600}) values obtained from untreated cells using the following formulas: inactivation of SOD, (absorbance value after treatment − absorbance value of untreated control)/OD_{600}; inactivation of CAT, (fluorescent value after treatment − fluorescent value of untreated control)/OD_{600}; inactivation of GPx, (fluorescent value of untreated control − fluorescent value after treatment)/OD_{600}.

have both enzymatic and nonenzymatic defense systems that can scavenge ROS. The most well-known nonenzymatic defense system, glutathione (GSH), is oxidized by ROS to oxidized glutathione (GSSG) and, thus, acts as a scavenger to protect cells from oxidative damage (58). On the other hand, the major enzymatic ROS defense systems include superoxide dismutase (SOD), catalase (CAT), and glutathione peroxidase (GPx) (59, 60). SOD is one of the most fundamental antioxidant enzymes and converts superoxide into hydrogen peroxide, which has less biological oxidant potential, and hydrogen peroxide is further decomposed by CAT to ground-state oxygen and water (61, 62). GPx catalyzes the reduction of hydrogen peroxide as well as a wide range of lipid hydroperoxides using GSH as a reductant (63). That is, several ROS defense systems of the organism scavenge ROS, maintaining low levels of ROS within the cell and protecting cells from oxidative cellular damage. Thus, the cells being exposed to unfavorable stresses and these defense systems becoming damaged and less effective can result in increased oxidative damage and eventually adversely affect the cell (64–67). Meanwhile, in our previous study (23), we demonstrated that the 222-nm KrCl excilamp inactivates the cellular enzyme respiratory chain dehydrogenase through photoinduced damage. From this result, therefore, we postulate that the synergistic increase in ROS generation by simultaneous 254-nm LP Hg lamp and 222-nm KrCl excilamp treatment was related especially to the enzymatic ROS defense system in the cell. Accordingly, the activities of SOD, CAT, and GPx, which are considered to be primary antioxidant enzyme families, were examined after treatment. As shown in Table 6, for both SOD and CAT, inactivation values of these enzymes were not significantly ($P > 0.05$) different from those of the untreated control after 254-nm LP Hg lamp treatment, but the values for 222-nm KrCl excilamp treatment and the combined 254-nm LP Hg lamp and 222-nm KrCl excilamp treatment were significantly ($P < 0.05$) higher than for that of the untreated control. Moreover, there were no significant ($P > 0.05$) differences between 222-nm KrCl excilamp treatment and the combination treatment of the 222-nm KrCl excilamp and 254-nm LP Hg lamp. In other words, the 254-nm LP Hg lamp treatment cannot inactivate either enzyme (SOD and CAT), whereas

222-nm KrCl excilamp treatment can inactivate both SOD and CAT, and simultaneous treatment with the 222-nm KrCl excilamp and 254-nm LP Hg lamp shows the same inactivation ability as individual treatment with the 222-nm KrCl excilamp for both SOD and CAT. Meanwhile, in the case of GPx utilizing 254-nm LP Hg lamp as well as 222-nm KrCl excilamp treatment, enzyme inactivation values were significantly ($P < 0.05$) increased compared to those of untreated controls. In addition, inactivation values were at the highest level of significance ($P < 0.05$) for the combination treatment, followed by the 222-nm KrCl excilamp and lastly by the 254-nm LP Hg lamp single treatments. This indicates that not only the 222-nm KrCl excilamp but also the 254-nm LP Hg lamp has inactivating capability against GPx. Furthermore, in the case of SOD and CAT, the degrees of enzyme inactivation were not significantly ($P > 0.05$) different between 222-nm KrCl excilamp and combination treatment, whereas in the case of GPx, the inactivation level of GPx after combination treatment was significantly ($P < 0.05$) higher than that of single 222-nm KrCl excilamp treatment. This can be interpreted as the result of additional effects, because the 254-nm LP Hg lamp has inactivation capability against GPx. These results indicate that the 222-nm KrCl excilamp exhibits inactivation ability against ROS defense enzymes, while the 254-nm LP Hg lamp did not exhibit inactivation ability for ROS defense enzymes such as SOD and CAT, and even though it showed inactivation ability for GPx, it was less effective than the 222-nm KrCl excilamp. It has been well established that the 222-nm wavelength has greater inactivation ability against enzymes in the solution as well as within cells than the 254-nm wavelength (23, 68, 69). This difference in enzyme response between 254-nm and 222-nm wavelengths is due to the larger absorption of light by proteins at 222 nm than at 254 nm. This occurs because the maximum wavelengths corresponding to absorption by major amino acids such as Tyr, Typ, Phe, His, and Cys are all under 240 nm (44, 70). That is, more absorption of 222-nm-wavelength light emitted by the KrCl excilamp than of 254-nm wavelength emitted by the LP Hg lamp led to more photoinduced reactions, resulting in greater photoinactivation damage.

In this study, total ROS and superoxide were not generated by 254-nm LP Hg lamp but only by 222-nm KrCl excilamp treatment. However, it is generally known that any wavelengths in the UV region can induce the generation of excited-state species and radicals via photoionization, as these wavelengths are absorbed by chromophoric amino acids present in the protein (41, 44). Therefore, it is possible that ROS can also be generated by 254-nm LP Hg lamp as well as 222-nm KrCl excilamp treatment, although the degree of ROS generation depends on the degree of UV absorption. In this regard, in a study on the response of Chlorophyceae to UV-C light treatment (71), it was reported that superoxide significantly increased in cells following 254-nm LP Hg treatment. The reason why total ROS and superoxide were not produced by the 254-nm LP Hg lamp treatment in our study but were generated in the study of Kováčik et al. (71) is thought to be the much larger dose of UV radiation applied in their study. In other words, it can be interpreted that total ROS and superoxide appeared not to be generated by 254-nm LP Hg lamp treatment in our study because not enough UV dose was applied to overcome the activity of ROS defense enzymes (SOD, CAT, and GPx); thus, total ROS and superoxide generated by 254-nm-wavelength exposure were scavenged by ROS defense enzymes. In the case of GPx, although 254-nm LP Hg lamp treatment inactivated this enzyme and thereby decreased ROS scavenging ability, there were no ROS occurrences. From this, it can be interpreted that the enzyme was inactivated but ROS are not generated, because 254-nm LP Hg lamp irradiation energy was insufficient to overcome the threshold necessary to inactivate enough enzyme to generate ROS for GPx. Based on this principle, the results of our study, in which total ROS and superoxide are synergistically generated, are interpreted as the following: with 254-nm LP Hg lamp and 222-nm KrCl excilamp simultaneous application, the 222-nm wavelength inactivated SOD, CAT, and GPx, leaving ROS generated by the 254-nm wavelength to remain unscavenged; thus, more ROS was generated than the sum of that generated by individual treatments with the 254-nm LP Hg lamp and 222-nm KrCl excilamp.

To date, many researchers have studied the effect of microbial inactivation through the combination of wavelengths using excilamps, UV-LEDs, and LP Hg lamps (17–21). Among them, the wavelength combinations of 254/365 nm, 254/405 nm, 280/365 nm, 254/365 nm, and 222/254 nm showed synergistic effects of microbial inactivation, while the wavelength combinations of 265/280 nm, 254/310 nm, 280/310 nm, 265/280/310 nm, 260/280 nm, and 172/222 nm did not show the synergistic effect of microbial inactivation. Oguma et al. (19) suggested that the difference in the absence or presence of the synergistic effect of microbial inactivation according to wavelength combination is due to the difference in emission wavelengths. In other words, when two wavelengths with different microbial inactivation mechanisms are combined, one wavelength will enhance the inactivation effect of the other wavelength, producing synergistic effects. Indeed, in the study of Nakahashi et al. (20), it was demonstrated that the combination of UV-C/UV-A (254/365 nm) wavelengths showed a synergistic bactericidal effect, and its mechanism is that UV-A (365 nm) attenuates the DNA repair pathway, such as SOS response, inducing an increase of the bactericidal effect of UV-C (254 nm) and resulting in a synergistic effect. Our results showing synergistic bactericidal effects by promoting ROS generation at the 254-nm wavelength by inactivating ROS defense enzymes at the 222-nm wavelength are also in line with the previous interpretation. Therefore, when developing a microbial control system through a combination of wavelengths, it is important to consider trying a combination of wavelengths with different inactivation mechanisms.

In conclusion, this study demonstrates that simultaneous treatment with the 254-nm LP Hg lamp and 222-nm KrCl excilamp exhibits a synergistic bactericidal effect on pathogenic bacteria present in tap water. This means that simultaneous treatment with both types of lamps can control bacteria more effectively by inputting the same energy as individual treatments with both wavelengths. Therefore, it is suggested that simultaneous 254-nm LP Hg lamp and 222-nm KrCl excilamp treatment has the potential to ensure greater water potability by applying this hurdle technology to the water disinfection process and improving the disinfection effect. The mechanism of this synergistic bactericidal action of the combination of these two wavelengths has been identified by several investigations. When the 254-nm LP Hg lamp and 222-nm KrCl excilamp are simultaneously applied, the ROS defense enzymes are inactivated by the 222-nm wavelength, resulting in additional ROS generation due to the 254-nm wavelength. This synergistic generation of ROS leads to the synergistic occurrence of lipid peroxidation of the cell membrane, resulting in synergistic physical damage in the form of pore formation in the cell membrane. Consequently, it has been shown that this synergistic bactericidal effect is produced by a series of chain reactions from inactivation of ROS enzymes to synergistic cell membrane damage. This finding will be an important basis for further development of disinfection systems combining the 254-nm LP Hg lamp and 222-nm KrCl excilamp and subsequent practical application by industry. This study also suggests further investigations into the application of combination treatments of the 222-nm KrCl excilamp with various oxidative agents, such as ozone, chlorine dioxide, hydrogen peroxide, and other similar compounds, because synergistic antimicrobial effect with oxidative agents can be anticipated based on the inactivation ability of the 222-nm KrCl excilamp against ROS defense enzymes revealed through this study.

MATERIALS AND METHODS

Bacterial strains and inoculum conditions. Three strains each of *E. coli* O157:H7 (ATCC 35150, ATCC 43889, and ATCC 43890), *S.* Typhimurium (ATCC 19585, ATCC 43971, DT 104), and *L. monocytogenes* (ATCC 19111, ATCC 19115, and ATCC 15313) were obtained from the bacterial culture collection of Seoul National University (Seoul, South Korea). Stock cultures were prepared by growing strains in 5 ml of tryptic soy broth (TSB; Difco, BD) at 37°C for 24 h, combining 0.7 ml with 0.3 ml of sterile 50% glycerol, and then storing at −80°C. Working cultures were streaked onto tryptic soy agar (TSA; Difco, BD), incubated at 37°C for 24 h, and stored at 4°C for less than 1 week.

Culture preparation and inoculation. Each strain of *E. coli* O157:H7, *S.* Typhimurium, and *L. monocytogenes* was cultured in 5 ml TSB at 37°C for 24 h, and then cell pellets were harvested by centrifugation at 4,000 × *g* for 20 min at 4°C and washed three times with sterile 0.2% peptone water
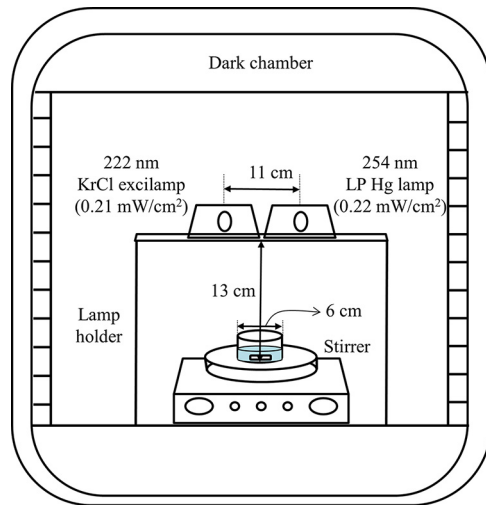
FIG 1 Schematic diagram of the combined 222-nm krypton-chlorine (KrCl) excilamp and 254-nm low-pressure mercury (LP Hg) lamp water treatment system used in this study.

(PW; Bacto, Sparks, MD). The final pellets were resuspended in 10 ml sterile tap water, corresponding to approximately 10^8 to 10^9 CFU/ml. The resuspended pellets of each strain of all pathogen taxa were combined to constitute a mixed culture cocktail because the simultaneous inoculation of several strains or pathogens becomes more similar to the realistic conditions (72).

To prepare water samples for treatment in the batch type water treatment system, 1 ml of mixed-culture cocktail was inoculated into 50 ml sterile tap water at room temperature, and then 5 ml of the inoculated tap water was transferred to a petri dish (60 mm by 15 mm).

Experimental setup and treatment. A DBD excilamp (20 W; 29 by 9 by 8 cm; UNILAM, Ulsan, South Korea) filled with a KrCl gas mixture and a conventional LP Hg lamp (16 W; G10T5/4P; 357 mm; Sankyo, Japan) were used as 222- and 254-nm UV irradiation sources, respectively. The DBD excilamp and LP Hg lamp were placed in a metal case with an aluminum reflector with an UV exit window of 60-cm² (10 cm by 6 cm) area. The two lamps were mounted side by side onto a stainless steel holder so that the sample was placed vertically in the middle of both lamps, and the distance from the middle point between the two emitters to the sample was 13 cm. With the two lamps configured in this way, radiation intensities were measured with an UV fiber optic spectrometer (AvaSpec-ULS2048; Avantes, Eerbeek, Netherlands) calibrated to a range of 200 to 400 nm within the UV-C spectrum at the location where the sample was placed. At this time, in order to adjust the radiation intensities of the two lamps to similar levels, an LP Hg lamp having higher radiation intensity was covered with 6 sheets of polypropylene (PP) film (thickness, 0.05 mm), and radiation intensities of the KrCl excilamp and LP Hg lamp were 0.21 and 0.22 mW/cm², respectively. The UV intensity was measured each day before performing experiments to confirm that constant intensity values were obtained. As a result, these intensity values showed an error range within ±0.005 mW/cm², indicating a constant value.

For UV-C treatment, a petri dish (60 by 15 mm²) containing 5 ml of the inoculated water sample described previously was placed on a magnetic stirrer (TM-17R; Jeio Tech, Daejeon, South Korea) and continuously mixed at 250 rpm for even irradiation. Prior to treatment, the UV lamps were turned on for about 15 min to stabilize. The samples were treated with the 222-nm KrCl excilamp or 254-nm LP Hg lamp or their combination for 1 to 15 s at equal doses of 0.21 to 3.15 mJ/cm² for the KrCl excilamp and 0.22 to 3.30 mJ/cm² for the LP Hg lamp at room temperature (22 ± 2°C) in a dark chamber. UV doses were calculated by multiplying values of light intensity by the irradiation times. A schematic diagram of the combined system of the 222-nm KrCl excilamp and 254-nm LP Hg lamp used in this experiment is shown in Fig. 1.

Bacterial enumeration. Following treatment, 1-ml aliquots of treated samples were 10-fold serially diluted in 9 ml of sterile 0.2% buffered peptone water, and 0.1-ml aliquots of samples or diluents were spread plated onto selective media. Xylose lysine desoxycholate agar (XLD; Difco), sorbitol MacConkey agar (SMAC; Difco), and Oxford agar base with Bacto Oxford antimicrobial supplement (MOX; Difco) were used as selective media for the enumeration of S. Typhimurium, E. coli O157:H7, and L. monocytogenes, respectively. Where low numbers of surviving cells were anticipated, 250 μl of undiluted sample was plated onto each of four plates. All plates were incubated at 37°C for 24 to 48 h before counting, and colonies were enumerated and calculated as $\log_{10}$ CFU/ml.

Enumeration of sublethally injured cells. To enumerate injured cells of S. Typhimurium and L. monocytogenes, the overlay method was used (73). One-tenth-milliliter aliquots of appropriate dilutions were spread plated onto TSA (a nonselective medium) to facilitate repair of injured cells, and the plates were incubated at 37°C for 2 h to enable injured cells to recover. The resuscitation medium plates were then overlaid with 7 ml of the selective medium XLD or OAB for S. Typhimurium or L. monocytogenes, respectively. After the overlay was solidified, plates were incubated at 37°C for an additional 22 h, and then typical black colonies characteristic for each pathogen were counted.

In the case of injured *E. coli* O157:H7, phenol red agar base (Difco) with 1% sorbitol (SPRAB) was used (74). One-tenth-milliliter aliquots of appropriate dilutions were spread plated onto SPRAB, and the plates were incubated at 37°C for 24 h. After incubation, white colonies characteristic of *E. coli* O157:H7 were enumerated, and simultaneously, serological confirmation (RIM; *E. coli* O157:H7 latex agglutination test; Remel, Lenexa, KS, USA) was conducted on randomly selected presumptive *E. coli* O157:H7 colonies.

Analysis of synergistic inactivation mechanisms. For the mechanism analysis experiments, *S.* Typhimurium, *L. monocytogenes*, and *E. coli* O157:H7 cells were adjusted to an optical density at 600 nm (OD_{600}) of 0.3 in sterile tap water and treated with 222-nm KrCl excilamp, 254-nm LP Hg lamp, or their combination for 5 s at equal doses of 1.10 mJ/cm^2 for the LP Hg lamp and 1.05 mJ/cm^2 for the KrCl excilamp for *E. coli* O157:H7 and 15 s at equal doses of 3.30 mJ/cm^2 for the LP Hg lamp and 3.15 mJ/cm^2 for *S.* Typhimurium and *L. monocytogenes* under the same conditions as those described above.

(i) Investigation of cell membrane damage. To identify cell membrane damage following treatment, the fluorescent dye propidium iodine (PI; Sigma-Aldrich, USA) or diphenyl-1-pyrenylphosphine (DPPP; Sigma-Aldrich, USA) was used to quantitatively assess the change of cell membrane permeability or the incidence of peroxidation, respectively. PI, which binds to nucleic acids (DNA and RNA) and emits fluorescence, does not pass through the intact cell membrane (75). Thus, the degree of pore formation in the cell membrane can be evaluated by fluorescent value generated by PI binding with nucleic acids through the PI uptake assay (24). DPPP is nonfluorescent and selectively reacts with lipid hydroperoxide within the cell membrane due to its high lipophilic characteristic and is oxidized to fluorescent DPPP oxide (DPPP=O) (76). Thus, the extent of incidence of lipid peroxidation within the cell membrane can be determined from the fluorescent value produced by oxidation of DPPP (77, 78).

Following treatments, treated samples were incubated with PI or DPPP solution at a final concentration of 2.9 or 50 μM for 10 or 20 min at 37°C, respectively. After incubation, cells were collected by centrifugation at 10,000 $\times$ *g* for 10 min and washed twice with phosphate-buffered saline (PBS), and fluorescence was measured with a spectrofluorophotometer (Spectramax M2e; Molecular Devices, CA, USA) at excitation/emission wavelengths of 493/630 nm for PI uptake assay or 351/380 nm for DPPP assay.

(ii) Detection of total ROS and superoxide (O_2^-) generation. CM-H_2DCFD, a cellular probe, was used to measure intracellular ROS. This probe can easily penetrate the cell membrane, be hydrolyzed to form the dichlorofluorescin (DCFH) carboxylate anion in the cell, and then be converted to highly fluorescent 2',7'-dichlorofluorescein (DCF) upon oxidation by ROS (79–81). Thus, the degree of generation of intracellular ROS was determined from increasing fluorescence values of DCF.

Intracellular superoxide was detected using hydroethidine (HDE) oxidized to produce ethidium bromide by reacting with superoxide within the cells. Since this oxidative product becomes fluorescent when it intercalates into DNA, it can quantitatively assess the extent of intracellular superoxide generation through measurement of fluorescence value (82–85).

Treated cells were immediately incubated with CM-H_2DCFDA [5-(and-6)-chloromethyl-2',7'-dichlorodihydrofluorescein diacetate; Invitrogen] and HDE (Molecular Probes, ThermoFisher Scientific) at a final concentration of 5 μM for 15 and 30 min at 37°C to assess the generation of intracellular total ROS and superoxide, respectively. After incubation, cells were collected by centrifugation at 10,000 $\times$ *g* for 10 min and washed twice with PBS, and fluorescence was measured with a spectrofluorophotometer at excitation/emission wavelengths of 495/520 nm for total ROS assay and 518/605 nm for superoxide assay, respectively.

(iii) Measurement of inactivity of SOD, CAT, and GPx. After treatment, treated samples were centrifuged at 10,000 $\times$ *g* for 10 min (4°C) and washed twice with PBS buffer. Cells resuspended in PBS were disrupted in an ice bath six times (10 s on and 10 s off) using a sonicator and centrifuged at 10,000 $\times$ *g* for 10 min (4°C) to obtain the supernatant used for SOD activity assay. SOD, CAT, and GPx activity measurement was carried out using an SOD assay kit (WST; Sigma-Aldrich), Amplex Red CAT assay kit (Invitrogen), and GPx assay kit (Abcam) according to the manufacturer's instructions.

The principle of this assay is that the superoxide anion produced by the oxidation of xanthine by xanthine oxidase reacts with WST-1 to produce yellow-colored WST-1 formazan, which absorbs light at 450 nm. On the other hand, this WST-1 formazan production reaction is competitively inhibited by SOD degrading superoxide anion. Therefore, the inactivity of SOD can be measured indirectly by measuring the degree of production of WST-1 formazan. In the case of the CAT assay, catalase first decomposes H_2O_2 into water and oxygen, and then the Amplex Red reagent reacts with a 1:1 stoichiometry with any unreacted H_2O_2 in the presence of horseradish peroxidase (HRP) to produce resorufin, a highly fluorescent oxidant. Since the resorufin increases with decreasing catalase activity, the inactivity of CAT can be quantitated by an increased fluorescence signal. In the case of GPx, glutathione (GSH) is catalyzed to oxidized glutathione (GSSG) by GPx, and then the resulting GSSG is recycled to GSH and again reduced by glutathione reductase (GR) and NADPH. NADP$^+$, generated as a result of the recycling of GSSG, can be monitored using an NADP sensor that reacts with NADP$^+$ to generate a fluorescent product. Therefore, since the fluorescence signal is proportional to the GPx activity, inactivity of GPx can be measured by the decreased fluorescence signal.

Statistical analysis. All experiments were replicated three times. All experiments for pathogen inactivation were duplicate plated. All data were analyzed by the analysis of variance (ANOVA) procedure of SAS (version 9.4; SAS Institute, Inc., Cary, NC, USA), and mean values of log reduction of pathogens or fluorescence/absorbance values normalized for OD_{600} were separated using the least significant difference *t* test. Significant differences between values were determined using a probability (*P*) level of <0.05.

ACKNOWLEDGMENTS

REFERENCES

1. Brassard J, Guévremont É, Gagné M-J, Lamoureux L. 2011. Simultaneous recovery of bacteria and viruses from contaminated water and spinach by a filtration method. Int J Food Microbiol 144:565–568. https://doi.org/10.1016/j.ijfoodmicro.2010.11.015.
2. WHO/UNICEF. 2014. Progress on drinking water and sanitation: 2014 update. World Health Organization, Geneva, Switzerland.
3. WHO. 2015. Progress on sanitation and drinking water: 2015 update and MDG assessment. World Health Organization, Geneva, Switzerland.
4. Song K, Mohseni M, Taghipour F. 2016. Application of ultraviolet light-emitting diodes (UV-LEDs) for water disinfection: a review. Water Res 94:341–349. https://doi.org/10.1016/j.watres.2016.03.003.
5. Hijnen W, Beerendonk E, Medema GJ. 2006. Inactivation credit of UV radiation for viruses, bacteria and protozoan (oo)cysts in water: a review. Water Res 40:3–22. https://doi.org/10.1016/j.watres.2005.10.030.
6. Mori M, Hamamoto A, Takahashi A, Nakano M, Wakikawa N, Tachibana S, Ikehara T, Nakaya Y, Akutagawa M, Kinouchi Y. 2007. Development of a new water sterilization device with a 365 nm UV-LED. Med Biol Eng Comput 45:1237–1241. https://doi.org/10.1007/s11517-007-0263-1.
7. Aoyagi Y, Takeuchi M, Yoshida K, Kurouchi M, Yasui N, Kamiko N, Araki T, Nanishi Y. 2011. Inactivation of bacterial viruses in water using deep ultraviolet semiconductor light-emitting diode. J Environ Eng 137:1215–1218. https://doi.org/10.1061/(ASCE)EE.1943-7870.0000442.
8. Dotson AD, Rodriguez CE, Linden KG. 1 May 2012. UV disinfection implementation status in US water treatment plants. J Am Water Works Assoc https://doi.org/10.5942/jawwa.2012.104.0075.
9. Lubello C, Gori R, Nicese FP, Ferrini F. 2004. Municipal-treated wastewater reuse for plant nurseries irrigation. Water Res 38:2939–2947. https://doi.org/10.1016/j.watres.2004.03.037.
10. Pirnie M, Linden KG, Malley JP, Schmelling D. 2006. Ultraviolet disinfection guidance manual for the final long term 2 enhanced surface water treatment rule: EPA 815-R-06-007. U.S. EPA, Washington, DC.
11. Chen J, Loeb S, Kim J-H. 2017. LED revolution: fundamentals and prospects for UV disinfection applications. Environ Sci Water Res Technol 3:188–202. https://doi.org/10.1039/C6EW00241B.
12. Orlowska M, Koutchma T, Kostrzynska M, Tang J. 2015. Surrogate organisms for pathogenic O157: H7 and non-O157 Escherichia coli strains for apple juice treatments by UV-C light at three monochromatic wavelengths. Food Control 47:647–655. https://doi.org/10.1016/j.foodcont.2014.08.004.
13. Matafonova G, Batoev V. 2012. Recent progress on application of UV excilamps for degradation of organic pollutants and microbial inactivation. Chemosphere 89:637–647. https://doi.org/10.1016/j.chemosphere.2012.06.012.
14. Rahman S, Khan I, Oh DH. 2016. Electrolyzed water as a novel sanitizer in the food industry: current trends and future perspectives. Comp Rev Food Sci Food Safety 15:471–490. https://doi.org/10.1111/1541-4337.12200.
15. Leistner L. 2000. Basic aspects of food preservation by hurdle technology. Int J Food Microbiol 55:181–186. https://doi.org/10.1016/S0168-1605(00)00161-6.
16. Khan I, Tango CN, Miskeen S, Lee BH, Oh D-H. 2017. Hurdle technology: a novel approach for enhanced food quality and safety—a review. Food Control 73:1426–1444. https://doi.org/10.1016/j.foodcont.2016.11.010.
17. Ramsay IA, Niedziela J-C, Ogden ID. 2000. The synergistic effect of excimer and low-pressure mercury lamps on the disinfection of flowing water. J Food Prot 63:1529–1533. https://doi.org/10.4315/0362-028X-63.11.1529.
18. Beck SE, Ryu H, Boczek LA, Cashdollar JL, Jeanis KM, Rosenblum JS, Lawal OR, Linden KG. 2017. Evaluating UV-C LED disinfection performance and investigating potential dual-wavelength synergy. Water Res 109:207–216. https://doi.org/10.1016/j.watres.2016.11.024.
19. Oguma K, Kita R, Sakai H, Murakami M, Takizawa S. 2013. Application of UV light emitting diodes to batch and flow-through water disinfection systems. Desalination 328:24–30. https://doi.org/10.1016/j.desal.2013.08.014.
20. Nakahashi M, Mawatari K, Hirata A, Maetani M, Shimohata T, Uebanso T, Hamada Y, Akutagawa M, Kinouchi Y, Takahashi A. 2014. Simultaneous irradiation with different wavelengths of ultraviolet light has synergistic bactericidal effect on Vibrio parahaemolyticus. Photochem Photobiol 90:1397–1403. https://doi.org/10.1111/php.12309.
21. Chevremont A-C, Farnet A-M, Coulomb B, Boudenne J-L. 2012. Effect of coupled UV-A and UV-C LEDs on both microbiological and chemical pollution of urban wastewaters. Sci Total Environ 426:304–310. https://doi.org/10.1016/j.scitotenv.2012.03.043.
22. Gross A, Stangl F, Hoenes K, Sift M, Hessling M. 2015. Improved drinking water disinfection with UVC-LEDs for Escherichia coli and Bacillus subtilis utilizing quartz tubes as light guide. Water 7:4605–4621. https://doi.org/10.3390/w7094605.
23. Kang J-W, Kim S-S, Kang D-H. 2018. Inactivation dynamics of 222 nm krypton-chlorine excilamp irradiation on Gram-positive and Gram-negative foodborne pathogenic bacteria. Food Res Int 109:325–333. https://doi.org/10.1016/j.foodres.2018.04.018.
24. Ha J-W, Lee J-I, Kang D-H. 2017. Application of a 222-nm krypton-chlorine excilamp to control foodborne pathogens on sliced cheese surfaces and characterization of the bactericidal mechanisms. Int J Food Microbiol 243:96–102. https://doi.org/10.1016/j.ijfoodmicro.2016.12.005.
25. Cho M, Kim J, Kim JY, Yoon J, Kim J-H. 2010. Mechanisms of Escherichia coli inactivation by several disinfectants. Water Res 44:3410–3418. https://doi.org/10.1016/j.watres.2010.03.017.
26. Wang D, Oppenländer T, El-Din MG, Bolton JR. 2010. Comparison of the disinfection effects of vacuum-UV (VUV) and UV light on Bacillus subtilis spores in aqueous suspensions at 172, 222 and 254 nm. Photochem Photobiol 86:176–181. https://doi.org/10.1111/j.1751-1097.2009.00640.x.
27. Yin F, Zhu Y, Koutchma T, Gong J. 2015. Inactivation and potential reactivation of pathogenic Escherichia coli O157:H7 in apple juice following ultraviolet light exposure at three monochromatic wavelengths. Food Microbiol 46:329–335. https://doi.org/10.1016/j.fm.2014.08.015.
28. Brash DE. 1988. UV mutagenic photoproducts in Escherichia coli and human cells: a molecular genetics perspective on human skin cancer. Photochem Photobiol 48:59–66.
29. Slieman TA, Nicholson WL. 2000. Artificial and solar UV radiation induces strand breaks and cyclobutane pyrimidine dimers in Bacillus subtilis spore DNA. Appl Environ Microbiol 66:199–205. https://doi.org/10.1128/AEM.66.1.199-205.2000.
30. Fröls S, Gordon PM, Panlilio MA, Duggin IG, Bell SD, Sensen CW, Schleper C. 2007. Response of the hyperthermophilic archaeon Sulfolobus solfataricus to UV damage. J Bacteriol 189:8708–8718. https://doi.org/10.1128/JB.01016-07.
31. Hamamoto A, Mori M, Takahashi A, Nakano M, Wakikawa N, Akutagawa M, Ikehara T, Nakaya Y, Kinouchi Y. 2007. New water disinfection system using UVA light-emitting diodes. J Appl Microbiol 103:2291–2298. https://doi.org/10.1111/j.1365-2672.2007.03464.x.
32. Wu V. 2008. A review of microbial injury and recovery methods in food. Food Microbiol 25:735–744. https://doi.org/10.1016/j.fm.2008.04.011.
33. Ha J-W, Kang D-H. 2018. Effect of intermittent 222 nm krypton-chlorine excilamp irradiation on microbial inactivation in water. Food Control 90:146–151. https://doi.org/10.1016/j.foodcont.2018.02.025.

34. Kim S-J, Kim D-K, Kang D-H. 2016. Using UVC light-emitting diodes at wavelengths of 266 to 279 nanometers to inactivate foodborne pathogens and pasteurize sliced cheese. Appl Environ Microbiol 82:11–17. https://doi.org/10.1128/AEM.02092-15.

35. Choi DS, Park SH, Choi SR, Kim JS, Chun HH. 2015. The combined effects of ultraviolet-C irradiation and modified atmosphere packaging for inactivating Salmonella enterica serovar Typhimurium and extending the shelf life of cherry tomatoes during cold storage. Food Packaging Shelf Life 3:19–30. https://doi.org/10.1016/j.fpsl.2014.10.005.

36. Pagán R, Mackey B. 2000. Relationship between membrane damage and cell death in pressure-treated Escherichia coli cells: differences between exponential-and stationary-phase cells and variation among strains. Appl Environ Microbiol 66:2829–2834. https://doi.org/10.1128/AEM.66.7.2829-2834.2000.

37. Park I-K, Kang D-H. 2013. Effect of electropermeabilization by ohmic heating for inactivation of Escherichia coli O157:H7, Salmonella enterica serovar Typhimurium, and Listeria monocytogenes in buffered peptone water and apple juice. Appl Environ Microbiol 79:7122–7129. https://doi.org/10.1128/AEM.01818-13.

38. Kaneda T. 1991. Iso- and anteiso-fatty acids in bacteria: biosynthesis, function, and taxonomic significance. Microbiol Rev 55:288–302.

39. Gutteridge J. 1995. Lipid peroxidation and antioxidants as biomarkers of tissue damage. Clin Chem 41:1819–1828.

40. Matsuda N, Horikawa M, Wang L-H, Yoshida M, Okaichi K, Okumura Y, Watanabe M. 2000. Differential activation of ERK 1/2 and JNK in normal human fibroblast-like cells in response to UVC radiation under different oxygen tensions. Photochem Photobiol 72:334–339. https://doi.org/10.1562/0031-8655(2000)072<0334:DAOEAJ>2.0.CO;2.

41. Pattison DI, Davies MJ. 2006. Actions of ultraviolet light on cellular structures, p 131–157. In Bignold LP (ed), Cancer: cell structures, carcinogens and genomic instability. Springer, New York, NY.

42. Zeeshan M, Prasad S. 2009. Differential response of growth, photosynthesis, antioxidant enzymes and lipid peroxidation to UV-B radiation in three cyanobacteria. S Afr J Bot 75:466–474. https://doi.org/10.1016/j.sajb.2009.03.003.

43. Zhang X, Rosenstein BS, Wang Y, Lebwohl M, Wei H. 1997. Identification of possible reactive oxygen species involved in ultraviolet radiation-induced oxidative DNA damage. Free Radic Biol Med 23:980–985. https://doi.org/10.1016/S0891-5849(97)00126-3.

44. Bensasson R, Land E, Truscott T. 2013. Flash photolysis and pulse radiolysis: contributions to the chemistry of biology and medicine. Elsevier Academic Press, San Diego, CA.

45. Kramer B, Muranyi P. 2014. Effect of pulsed light on structural and physiological properties of Listeria innocua and Escherichia coli. J Appl Microbiol 116:596–611. https://doi.org/10.1111/jam.12394.

46. Joshi SG, Cooper M, Yost A, Paff M, Ercan UK, Fridman G, Friedman G, Fridman A, Brooks AD. 2011. Nonthermal dielectric-barrier discharge plasma-induced inactivation involves oxidative DNA damage and membrane lipid peroxidation in Escherichia coli. Antimicrob Agents Chemother 55:1053–1062. https://doi.org/10.1128/AAC.01002-10.

47. Lovrić J, Cho SJ, Winnik FM, Maysinger D. 2005. Unmodified cadmium telluride quantum dots induce reactive oxygen species formation leading to multiple organelle damage and cell death. Chem Biol 12:1227–1234. https://doi.org/10.1016/j.chembiol.2005.09.008.

48. von Moos N, Slaveykova VI. 2014. Oxidative stress induced by inorganic nanoparticles in bacteria and aquatic microalgae—state of the art and knowledge gaps. Nanotoxicology 8:605–630. https://doi.org/10.3109/17435390.2013.809810.

49. Wickens AP. 2001. Ageing and the free radical theory. Respir Physiol 128:379–391. https://doi.org/10.1016/S0034-5687(01)00313-9.

50. Gülçin İ. 2006. Antioxidant activity of caffeic acid (3,4-dihydroxycinnamic acid). Toxicology 217:213–220. https://doi.org/10.1016/j.tox.2005.09.011.

51. Halliwell B, Gutteridge J. 1984. Oxygen toxicity, oxygen radicals, transition metals and disease. Biochem J 219:1–14. https://doi.org/10.1042/bj2190001.

52. Yeware AM, Shurpali KD, Athalye MC, Sarkar D. 2017. Superoxide generation and its involvement in the growth of Mycobacterium smegmatis. Front Microbiol 8:105. https://doi.org/10.3389/fmicb.2017.00105.

53. Bielski B, Arudi RL, Sutherland MW. 1983. A study of the reactivity of HO2/O2 with unsaturated fatty acids. J Biol Chem 258:4759–4761.

54. Gogniat G, Dukan S. 2007. TiO2 photocatalysis causes DNA damage via Fenton reaction-generated hydroxyl radicals during the recovery period. Appl Environ Microbiol 73:7740–7743. https://doi.org/10.1128/AEM.01079-07.

55. Goulhen-Chollet F, Josset S, Keller N, Keller V, Lett M-C. 2009. Monitoring the bactericidal effect of UV-A photocatalysis: a first approach through 1D and 2D protein electrophoresis. Catal Today 147:169–172. https://doi.org/10.1016/j.cattod.2009.06.001.

56. Maness P-C, Smolinski S, Blake DM, Huang Z, Wolfrum EJ, Jacoby WA. 1999. Bactericidal activity of photocatalytic TiO2 reaction: toward an understanding of its killing mechanism. Appl Environ Microbiol 65:4094–4098.

57. Gogniat G, Thyssen M, Denis M, Pulgarin C, Dukan S. 2006. The bactericidal effect of TiO2 photocatalysis involves adsorption onto catalyst and the loss of membrane integrity. FEMS Microbiol Lett 258:18–24. https://doi.org/10.1111/j.1574-6968.2006.00190.x.

58. Sies H. 1999. Glutathione and its role in cellular functions. Free Radic Biol Med 27:916–921. https://doi.org/10.1016/S0891-5849(99)00177-X.

59. Li L, Ng T, Song M, Yuan F, Liu Z, Wang C, Jiang Y, Fu M, Liu F. 2007. A polysaccharide–peptide complex from abalone mushroom (Pleurotus abalonus) fruiting bodies increases activities and gene expression of antioxidant enzymes and reduces lipid peroxidation in senescence-accelerated mice. Appl Microbiol Biotechnol 75:863–869. https://doi.org/10.1007/s00253-007-0865-4.

60. Thirumalai T, David E, Therasa SV, Elumalai E. 2011. Restorative effect of Eclipta alba in CCl4 induced hepatotoxicity in male albino rats. Asian Pacific J Trop Dis 1:304–307. https://doi.org/10.1016/S2222-1808(11)60072-8.

61. McCord JM, Fridovich I. 1969. Superoxide dismutase an enzymic function for erythrocuprein (hemocuprein). J Biol Chem 244:6049–6055.

62. Nakonieczna J, Michta E, Rybicka M, Grinholc M, Gwizdek-Wiśniewska A, Bielawski KP. 2010. Superoxide dismutase is upregulated in Staphylococcus aureus following protoporphyrin-mediated photodynamic inactivation and does not directly influence the response to photodynamic treatment. BMC Microbiol 10:323. https://doi.org/10.1186/1471-2180-10-323.

63. Galiazzo F, Schiesser A, Rotilio G. 1987. Glutathione peroxidase in yeast. Presence of the enzyme and induction by oxidative conditions. Biochem Biophys Res Commun 147:1200–1205. https://doi.org/10.1016/S0006-291X(87)80197-3.

64. Santos AL, Oliveira V, Baptista I, Henriques I, Gomes NC, Almeida A, Correia A, Cunha Â. 2013. Wavelength dependence of biological damage induced by UV radiation on bacteria. Arch Microbiol 195:63–74. https://doi.org/10.1007/s00203-012-0847-5.

65. Sun H, Li G, Nie X, Shi H, Wong P-K, Zhao H, An T. 2014. Systematic approach to in-depth understanding of photoelectrocatalytic bacterial inactivation mechanisms by tracking the decomposed building blocks. Environ Sci Technol 48:9412–9419. https://doi.org/10.1021/es502471h.

66. Xia D, Ng TW, An T, Li G, Li Y, Yip HY, Zhao H, Lu A, Wong P-K. 2013. A recyclable mineral catalyst for visible-light-driven photocatalytic inactivation of bacteria: natural magnetic sphalerite. Environ Sci Technol 47:11166–11173. https://doi.org/10.1021/es402170b.

67. Xia D, Shen Z, Huang G, Wang W, Yu JC, Wong PK. 2015. Red phosphorus: an earth-abundant elemental photocatalyst for "green" bacterial inactivation under visible light. Environ Sci Technol 49:6264–6273. https://doi.org/10.1021/acs.est.5b00531.

68. Clauß M, Grotjohann N. 2008. Effective photoinactivation of alpha-amylase, catalase and urease at 222 nm emitted by an KrCl-excimer lamp. Clean Soil Air Water 36:754–759. https://doi.org/10.1002/clen.200700184.

69. Clauss M, Springorum AC, Hartung J. 2009. Ultraviolet disinfection with 222 nm wavelength—new options to inactivate UV-resistant pathogens. In Sustainable animal husbandry: prevention is better than cure, vol 2. Proc 14th Int Congr Int Soc Anim Hyg (ISAH), Vechta, Germany, 19 to 23 July 2009.

70. Kerwin BA, Remmele RL. 2007. Protect from light: photodegradation and protein biologics. J Pharm Sci 96:1468–1479. https://doi.org/10.1002/jps.20815.

71. Kováčik J, Klejdus B, Bačkor M. 2010. Physiological responses of Scenedesmus quadricauda (Chlorophyceae) to UV-A and UV-C light. Photochem Photobiol 86:612–616. https://doi.org/10.1111/j.1751-1097.2010.00708.x.

72. Jeong S-G, Kang D-H. 2017. Inactivation of Escherichia coli O157:H7, Salmonella Typhimurium, and Listeria monocytogenes in ready-to-bake cookie dough by gamma and electron beam irradiation. Food Microbiol 64:172–178. https://doi.org/10.1016/j.fm.2016.12.017.

73. Lee S-Y, Kang D-H. 2001. Suitability of overlay method for recovery of

heat-injured Listeria monocytogenes and Salmonella Typhimurium. Food Sci Biotechnol 10:323–326.

74. Hee M-S, Lee S-Y, Hillers VN, McCurdy SM, Kang D-H. 2003. Evaluation of consumer-style cooking methods for reduction of Escherichia coli O157:H7 in ground beef. J Food Prot 66:1030–1034.

75. Breeuwer P, Abee T. 2000. Assessment of viability of microorganisms employing fluorescence techniques. Int J Food Microbiol 55:193–200. https://doi.org/10.1016/S0168-1605(00)00163-X.

76. Okimoto Y, Watanabe A, Niki E, Yamashita T, Noguchi N. 2000. A novel fluorescent probe diphenyl-1-pyrenylphosphine to follow lipid peroxidation in cell membranes. FEBS Lett 474:137–140. https://doi.org/10.1016/S0014-5793(00)01587-8.

77. Tanaka T, Shimoda M, Shionoiri N, Hosokawa M, Taguchi T, Wake H, Matsunaga T. 2013. Electrochemical disinfection of fish pathogens in seawater without the production of a lethal concentration of chlorine using a flow reactor. J Biosci Bioeng 116:480–484. https://doi.org/10.1016/j.jbiosc.2013.04.013.

78. Boylan JA, Gherardini FC. 2008. Determining the cellular targets of reactive oxygen species in Borrelia burgdorferi, p 213–221. In Nordenfelt P, Collin M (ed), Bacterial pathogenesis. Springer, New York, NY.

79. Wojtala A, Bonora M, Malinska D, Pinton P, Duszynski J, Wieckowski MR. 2014. Methods to monitor ROS production by fluorescence microscopy and fluorometry. Methods Enzymol 542:243–262. https://doi.org/10.1016/B978-0-12-416618-9.00013-3.

80. Negre-Salvayre A, Augé N, Duval C, Robbesyn F, Thiers J-C, Nazzal D, Benoist H, Salvayre R. 2002. Detection of intracellular reactive oxygen species in cultured cells using fluorescent probes. Methods Enzymol 352:62–71. https://doi.org/10.1016/S0076-6879(02)52007-3.

81. Kalyanaraman B, Darley-Usmar V, Davies KJ, Dennery PA, Forman HJ, Grisham MB, Mann GE, Moore K, Roberts LJ, Ischiropoulos H. 2012. Measuring reactive oxygen and nitrogen species with fluorescent probes: challenges and limitations. Free Radic Biol Med 52:1–6. https://doi.org/10.1016/j.freeradbiomed.2011.09.030.

82. Yoshihisa Y, Honda A, Zhao QL, Makino T, Abe R, Matsui K, Shimizu H, Miyamoto Y, Kondo T, Shimizu T. 2010. Protective effects of platinum nanoparticles against UV-light-induced epidermal inflammation. Exp Dermatol 19:1000–1006. https://doi.org/10.1111/j.1600-0625.2010.01128.x.

83. Marcén M, Ruiz V, Serrano MJ, Condón S, Mañas P. 2017. Oxidative stress in E. coli cells upon exposure to heat treatments. Int J Food Microbiol 241:198–205. https://doi.org/10.1016/j.ijfoodmicro.2016.10.023.

84. Gomes A, Fernandes E, Lima JL. 2005. Fluorescence probes used for detection of reactive oxygen species. J Biochem Biophys Methods 65:45–80. https://doi.org/10.1016/j.jbbm.2005.10.003.

85. Hassan HM, Fridovich I. 1979. Intracellular production of superoxide radical and of hydrogen peroxide by redox active compounds. Arch Biochem Biophys 196:385–395. https://doi.org/10.1016/0003-9861(79)90289-3.